CHAPTER 7

Al-Zn Substituted $SrFe_{8-x}Al_4Zn_xO_{19}$ Series

7.1 Introduction

High coercivity (H_c) can be realized by many phenomena, as listed in Table 7.1 (Lewis & Jiménez-Villacorta, 2013). The dependency of H_c value on these phenomena and on the grain size distribution may result in a huge variation in the magnetic properties of SrM with the compositional elements. Based on the results of chapter 5, the 4 Al^{3+} ion substitution in SrM hexaferrite is further studied in this chapter with the substitution of Zn^{2+} ion at Fe lattice site. The drawback of four Al-substitution is tried to compensate with Zn ion to improve the magnetic properties because, in $SrFe_{11}ZnO_{19}$ composition, a high M_s of 77.9 emu/g is achieved, which is even higher than the maximum theoretical M_s value of SrM (~72 emu/g). In the present chapter, a composition of $SrFe_{8-x}Al_4Zn_xO_{19}$ (x = 0, 0.2, 0.4, 0.6, 0.8, 1) is ascertained, and the feasibility of enhancing magnetic properties in strontium hexaferrite has been further studied.

Table 7.1 *Different phenomena and sources of magnetic anisotropy to tailor the coercive field of material.*

Phenomenon	Source
Magnetocrystalline anisotropy	Spin-orbit interaction intrinsic to the specific crystal structure
Stress anisotropy or magnetostriction	Product of spin-orbit interaction, Arises from strain dependence of anisotropy constant
Shape anisotropy	Stray fields minimization through magnetization alignment with acicular axes in macroscopic particles
Exchange anisotropy	Quantum mechanical exchange at ferro/antiferromagnetic interface
Pinning of domain walls	Obstruction of magnetic domain wall motion by inclusion

7.2 Results and Discussion

7.2.1 Structural Properties

Fig. 7.1 shows the x-ray diffraction (XRD) patterns of auto-combustion synthesized $SrFe_{8-x}Al_4Zn_xO_{19}$ ($0 \leq x \leq 1$) calcined powder. All the resilient XRD peaks matched with the strontium hexaferrite peaks of ICDD card no. 79-1411 and indexed accordingly. The absence of any additional phase in the measuring range confirms the formation of pure and well-crystallized hexagonal phases with space group of $P6_3/mmc$. The values of structural parameters are listed in Table 7.2.

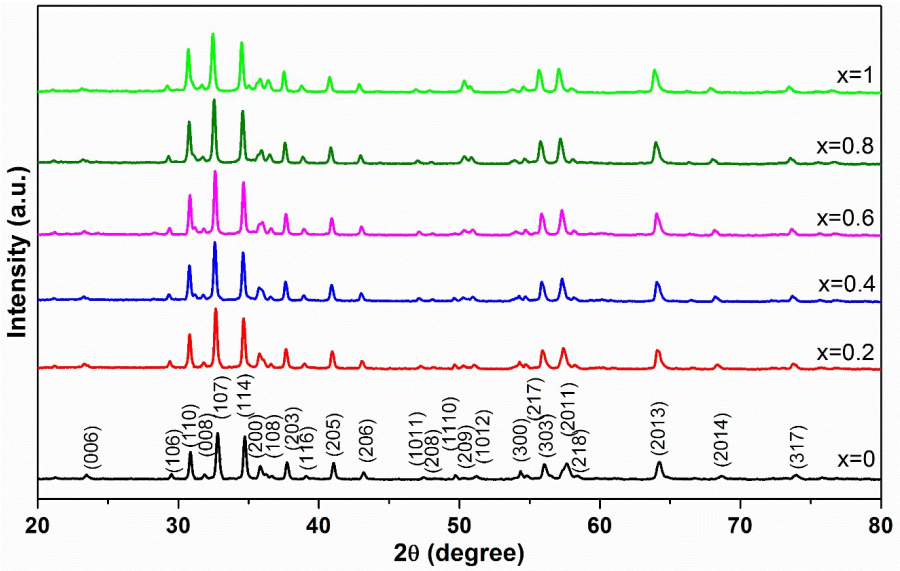

Figure 7.1 *XRD patterns of $SrFe_{8-x}Al_4Zn_xO_{19}$ ($0 \leq x \leq 1$) hexaferrites.*

The lattice parameters (*a* & *c*) are found to increase with the Zn^{2+} ion content, where an increase in *a* is almost steady while the change in *c* is significant. Steeper variation in *c* parameter points out the change in easy demagnetization axis. Due to the larger ionic radius of Zn^{2+} (0.74 Å) ion than Fe^{3+} (0.67 Å) ion (Liu et al., 2019a), the substitution of Zn ion causes the resultant ionic radius change of $\Delta r = +0.07$ Å, which is responsible for such kind of varying trend in lattice parameters. The increasing behavior of lattice parameters validates the effective substitution of Zn ion at Fe lattice site into the SrM structure.

Verstegen *et al.* (1974) have proposed that the *c/a* ratio can tell about the structure type (Stingaciu et al., 2021). The *c/a* ratio less than 3.98 approves the formation of magnetoplumbite hexagonal structure of all samples. The average crystallite size (*D*) is found in 30-47 nm range. It also endorses the formation of single-domain particles as it is lesser to a huge extent than the critical single domain size of ~500 nm for pure strontium hexaferrite driven by Kittle's theory of single domain creation (Luo et al., 2012). The unit-cell volume (*V*) is observed to increase due to the substitution of smaller Fe ions by larger Zn ions, which results in the increment of x-ray density.

Table 7.2 *Structural parameters of $SrFe_{8-x}Al_4Zn_xO_{19}$ ($0 \leq x \leq 1$) hexaferrites.*

Composition	Lattice Parameter		*c/a*	*V*	*D*	*Є*	*χD*
	***a, b* (Å)**	***c* (Å)**		**(Å^3)**	**(nm)**	**(10^{-3})**	**(g/cm^3)**
x=0	5.80	22.74	3.92	662.49	30.65	3.79	4.744
x=0.2	5.81	22.90	3.94	669.45	32.16	3.62	4.704
x=0.4	5.81	22.93	3.95	670.33	35.38	3.30	4.707
x=0.6	5.81	22.93	3.95	670.33	43.00	2.71	4.717
x=0.8	5.81	22.99	3.96	672.08	44.28	2.63	4.714
x=1	5.82	23.06	3.96	676.45	46.21	2.53	4.693

7.2.2 Spectroscopic Properties

FT-IR spectroscopy of desiccated calcined powder of $SrFe_{8-x}Al_4Zn_xO_{19}$ ($0 \leq x \leq 1$) in the range of 4000-400 cm^{-1} are shown in Fig. 7.2. In M-type hexaferrite, three absorption peaks generally appeared in the range of 400-700 cm^{-1} (Mali & Ataie, 2005). These peaks are related to the stretching vibration of Fe–O bonds at octahedral lattice sites (appeared in the 400-500 cm^{-1} range) and tetrahedral lattice sites (appeared in the 500-700 cm^{-1} range) (Baniasadi et al., 2014).

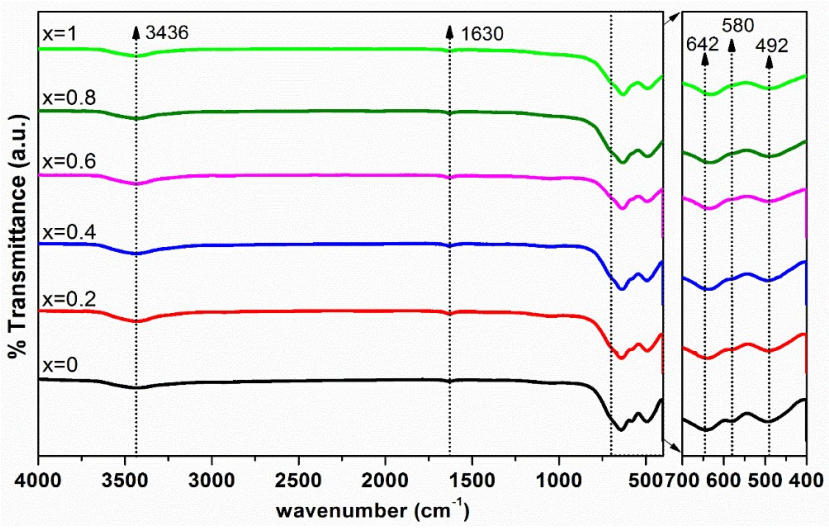

Figure 7.2 *FT-IR spectra of calcined $SrFe_{8-x}Al_4Zn_xO_{19}$ ($0 \leq x \leq 1$) hexaferrites.*

Table 7.3 *Characteristic absorption peaks [ν_1, ν_2 (tetrahedral) & ν_3 (octahedral)] and bond length (r) of $SrFe_{8-x}Al_4Zn_xO_{19}$ ($0 \leq x \leq 1$) hexaferrites.*

Composition	ν_1 (cm^{-1})	r_1 (Å)	ν_2 (cm^{-1})	r_2 (Å)	ν_3 (cm^{-1})	r_3 (Å)
x=0	642	4.21	581	4.50	494	5.01
x=0.2	640	4.22	581	4.50	492	5.03
x=0.4	638	4.23	581	4.50	492	5.03
x=0.6	635	4.24	0	-	491	5.03
x=0.8	632	4.25	0	-	490	5.04
x=1	630	4.26	0	-	490	5.04

According to Table 7.3, all obtained absorption peaks are in the 400-700 cm^{-1} range, which confirms the formation of M-type strontium hexaferrite. Additionally, two peaks at 1630 cm^{-1} and 3436 cm^{-1} are observed in all samples, which represents the stretching and deformation vibration of the hydroxy group (–OH) assimilated by the moist atmosphere (Xie et al., 2014). In the FTIR spectrum, shifting of characteristic absorption peaks [ν_1, ν_2 (tetrahedral) & ν_3 (octahedral)] is associated with Hooke's law, which states that a reverse relationship exists among wavenumbers and the atomic weight of molecules. It is observed that ν_2 peak is nearly become indistinguishable in the compositions with higher Zn content

($x \geq 0.6$) due to the shifting of resilient absorption peaks. Similar indistinguishable peak shifting due to Zn ion substitution is also observed by (Baniasadi et al., 2014). Replacement of the Fe ion (55.85 g/mol) with the heavier Zn ion (65.38 g/mol) causes the shifting of resilient peaks towards the lower wavenumber, according to Hooke's law. The dominant shifting of ν_1 band indicates the substitutional preference of Zn^{2+} ion to the tetrahedral lattice site of Fe^{3+} ion. It confirms the involvement of substituted ions in the strontium hexaferrite structure.

7.2.3 Densification and Microstructural Properties

The density of all the compositions is estimated by Archimedes' methodology and listed in Table 7.4, along with the porosity. The density of magnetic materials positively favors the improvement of saturation magnetization in strontium hexaferrite systems (Rawlings, 2009). Hence, in order to improve the magnetic parameters, low melting Zn ion is substituted to increase the density of Al-substituted strontium hexaferrite magnets. The substitution of Zn ion is observed to densify the samples. Melting temperature of the Zn ion is ~420°C, which helps to improve the density by dissolving with high solubility in the SrM structure and promotes grain growth in sintered pellets. Furthermore, EDS measurement confirms the presence of Sr, Fe, Al, Zn and O elements respective to the composition, and their atomic weight percentage are listed in Table 7.4.

Fig. 7.3 shows SEM micrograph of $SrFe_{8-x}Al_4Zn_xO_{19}$ ($0 \leq x \leq 1$) hexaferrites. These micrographs confirm the formation of hexagonal platelet-like morphology in all samples. The average grain size is found to increase with the increasing content of Zn^{2+} ions and is shown in Table 7.4. The substitution of different elements may improve the grain growth or work as the grain growth inhibitor depending on their interacting nature with the particle's boundary or defects in the lattice. Al ion works as a grain-growth inhibitor (Rhein et al., 2017). Al ion inhibits grain growth due to the diffusion process that plays a significant

Table 7.4 *Atomic weight %, average grain size (G_{avg}), bulk density (BD), and porosity (P) of $SrFe_{12-x-y}Ni_xAl_yO_{19}$ ($0.005 \leq x \leq 0.02$; $1 \leq y \leq 4$) hexaferrites.*

Composition	Atomic weight %					G_{avg}	*BD*	Porosity
	Sr	Fe	Al	Zn	O	(µm)	(g/cm^3)	(%)
x=0	5.69	40.27	11.02	-	43.02	0.74	3.53	25.59
x=0.2	5.64	39.91	10.94	1.19	42.32	1.53	4.33	7.95
x=0.4	5.59	39.58	10.87	2.53	41.43	1.97	4.39	6.73
x=0.6	5.53	38.88	10.76	3.95	40.88	2.37	4.41	6.51
x=0.8	5.48	38.14	10.63	5.11	40.64	2.68	4.49	4.75
x=1	5.39	37.45	10.58	6.19	40.39	2.75	4.48	4.54

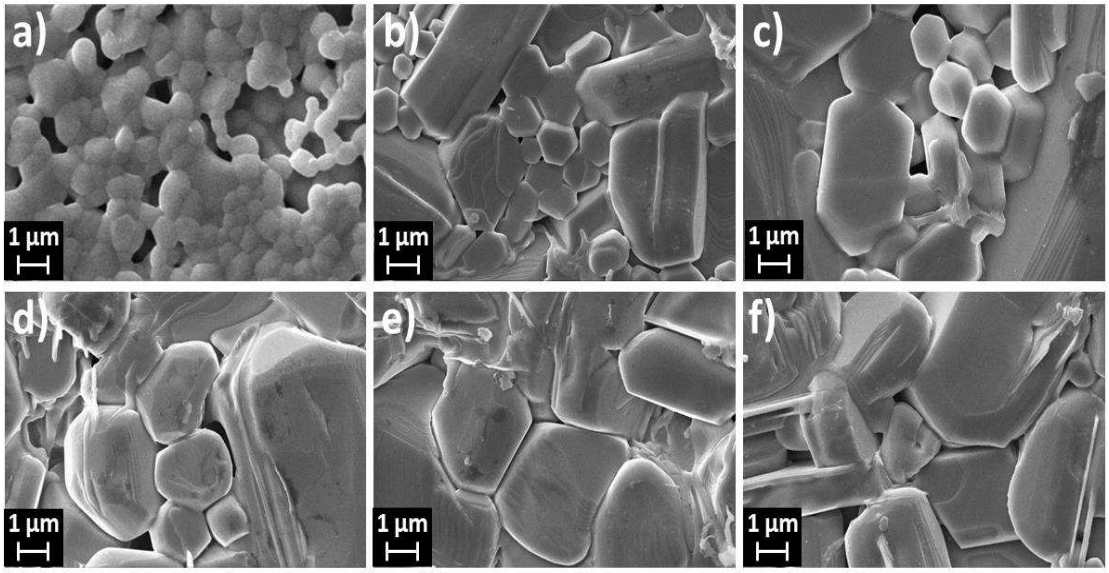

Figure 7.3 *SEM micrographs of a) $SrFe_8Al_4O_{19}$, b) $SrFe_{7.8}Al_4Zn_{0.2}O_{19}$, c) $SrFe_{7.6}Al_4Zn_{0.4}O_{19}$, d) $SrFe_{7.4}Al_4Zn_{0.6}O_{19}$, e) $SrFe_{7.2}Al_4Zn_{0.8}O_{19}$, and f) $SrFe_7Al_4ZnO_{19}$ hexaferrites.*

role in inhibiting the movement of domain walls (Rianna et al., 2019). The increase in the grain size is observed because of the upgrading mobility of grain boundary due to the Zn substitution (Kumar Godara et al., 2022). As the sintering process proceeds, nonstationary grain growth occurs and the grain growth mechanism depend on three types of grains: growing, stagnant, and dissolving (Kang et al., 2009). The driving force is mostly the average particle size for coarsening in a system because the driving force for growth and

dissolution is proportional to the curvature difference between average grain size and the size of a concerned grain. It may be possible that there are small no. of grains whose driving force is greater than the critical value of driving force, then these grain will grow considerably at the expense of other small grains which does not have enough driving force for grain growth (Jung et al., 2009). It leads to excessive grain growth in the system. The low melting point ~420°C of Zn element and high sintering temperature contributes to the exaggerated grain growth by liquid phase assisted sintering process and results in the massive increase of average grain size.

7.2.4 Magnetic Properties

Fig. 7.4 shows magnetic hysteresis loops of $SrFe_{8-x}Al_4Zn_xO_{19}$ ($0 \leq x \leq 1$) sintered pellets at 300 K, and different magnetic parameters are listed in Table 7.5. The saturation magnetization (M_s) is observed in the range of 14.88-25.54 emu/g, and remanent magnetization (M_r) is in the range of 8.04-12.73 emu/g. Coercivity (H_c) of compositions is obtained in the 9.30-17.93 kOe range.

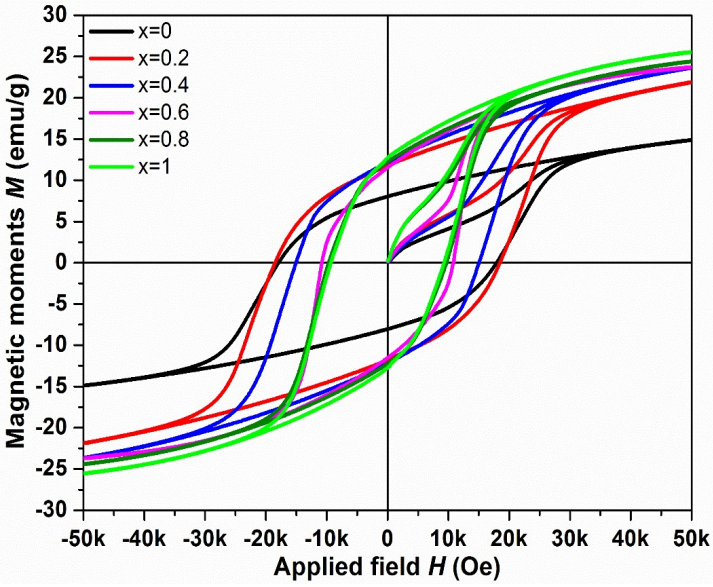

Figure 7.4 *M-H hysteresis curve of $SrFe_{8-x}Al_4Zn_xO_{19}$ ($0 \leq x \leq 1$) hexaferrites.*

Table 7.5 *Saturation magnetization (M_s), remanent magnetization (M_r), squareness ratio (M_r/M_s), coercivity (H_c), magnetocrystalline anisotropy field (H_a), and effective magnetic anisotropy (K_{eff}) of $SrFe_{8-x}Al_4Zn_xO_{19}$ ($0 \leq x \leq 1$) hexaferrites at 300 K.*

Composition	M_s (emu/g)	M_r (emu/g)	$\frac{M_r}{M_s}$	μ_B	H_c (kOe)	H_a (kOe)	K_{eff} (10^5 erg/g)
$SrFe_8Al_4O_{19}$	14.88	8.04	0.54	2.52	17.93	27.78	2.07
$SrFe_{7.8}Al_4Zn_{0.2}O_{19}$	21.87	11.80	0.54	3.71	18.51	27.20	2.97
$SrFe_{7.6}Al_4Zn_{0.4}O_{19}$	23.63	12.21	0.52	4.02	15.04	26.85	3.17
$SrFe_{7.4}Al_4Zn_{0.6}O_{19}$	23.71	11.53	0.49	4.04	10.83	26.84	3.18
$SrFe_{7.2}Al_4Zn_{0.8}O_{19}$	24.40	12.25	0.50	4.17	9.70	26.61	3.25
$SrFe_7Al_4ZnO_{19}$	25.54	12.73	0.50	4.37	9.30	25.70	3.28

In strontium hexaferrite structure, Fe ions are distributed at five different lattice sites having different spin-direction, which are three octahedral sites *12k* (↑), *2a* (↑), *4f₂* (↓), one tetrahedral site *4f₂* (↑), and one trigonal bipyramidal site *2b* (↑). These lattice sites play a significant role in the magnetism of strontium hexaferrite due to the superexchange interaction coupling among Fe^{3+} ions through O^{2-} ions (Slimani et al., 2020). If any less magnetic ion is substituted at Fe ($5\mu_B$) site, occupying tendency of substituted elements in up-spin moment direction sites will eventually decrease the M_s value while occupying preference of substituted elements towards down-spin direction will improve the M_s of material. According to the reported Mössbauer study, Al^{3+} ($0\mu_B$) ions possess occupying tendency towards the *12k* (↑) and *2a* (↑) lattice sites (Wang et al., 2012). Substitution of 4 Al^{3+} ions in SrM structure results in a small value of M_s due to reduction of net magnetic moment in up-spin directions and disturbed magnetic collinearity, which suppressed the superexchange interaction among Fe ions due to non-magnetic nature of substituted element (Liu et al., 2011). It reduces M_s value drastically to 14.88 emu/g in our composition, which is still better in comparison to other reported study (Luo et al., 2012; Trusov et al., 2018; Wang et al., 2012). According to the reported Mössbauer study, Zn^{2+}

($0\mu_B$) ions possess occupying tendency towards the *4f₁* (↓) and *2b* (↑) lattice sites (Banihashemi et al., 2021; Lee et al., 2005). The *2b* (↑) lattice site can show pseudo-tetrahedral character; hence it is reasonable for Zn^{2+} ion to occupy *2b* site also (Lee et al., 2005). The M_s value in $SrFe_{8-x}Al_4Zn_xO_{19}$ ($0 \leq x \leq 1$) composition is observed to increase continuously with the Zn content. Substitution of non-magnetic Zn ($0\mu_B$) ion have strong preference to tetrahedral site *4f₁* (↓) and results in an increase of net magnetic moment in up-spin direction. The increase in net magnetic moment contributes to the high M_s value as observed in the composition. The Bohr magneton number (μ_B) is found in an increasing manner with Zn content. The increase in μ_B is an other reason for increase in M_s. With the increasing amount of Zn substitution, improvement in M_s value is not very much evident. This might be due to the occupying preference of some Zn ions to the *2b* (↑) lattice site also and the deviation from collinear to non-collinear spin arrangement due to high content of Zn ions (Banihashemi et al., 2021; Zhang et al., 2021).

The remanent magnetization (M_r) is also increasing with the Zn ion content except for x = 0.6. It is an extrinsic property of a material and depends on M_s value, grain morphology, and synthesis parameters (Fersi et al., 2014). The character of *M-H* curve depends on the degree of magnetic anisotropy of particles and the orientation of easy axes concerning the applied field. The squareness ratio (M_r/M_s) gives information about the type of magnetic domain in a material. According to the Stoner-Wohlfarth (S-W) model, the squareness ratio is given by 0.5 in case of uniaxial anisotropy and 0.832 in case of cubic anisotropy in the materials having non-interacting random particle distribution (Topkaya, 2017). The squareness ratio is observed in the 0.49-0.54 range, which concludes the uniaxial anisotropy of particles along *c*-axis. $M_r/M_s \geq 0.5$ indicates single magnetic domain formation, while $M_r/M_s < 0.5$ specifies multi-magnetic domain formation in the system.

Coercivity is an extrinsic property of a material that mainly depends on the size of grains and magnetic anisotropy. The H_c of material exhibits a proportional relationship to the magnetocrystalline anisotropy field, and a similar variation trend of H_c is observed with H_a. Based on the Stoner-Wohlfarth (S-W) theory, the value of magnetocrystalline anisotropy field (H_a) and effective magnetocrystalline anisotropy (K_{eff}) are calculated by Eq. (2.14) [$K_{eff} = M_s\sqrt{(15\gamma/4)} = M_s H_a/2$] (Almessiere et al., 2019) and given in Table 4.4. The value of γ is obtained through the slope of S-W fitting of M vs. $1/H^2$ plot as shown in Fig. 7.5.

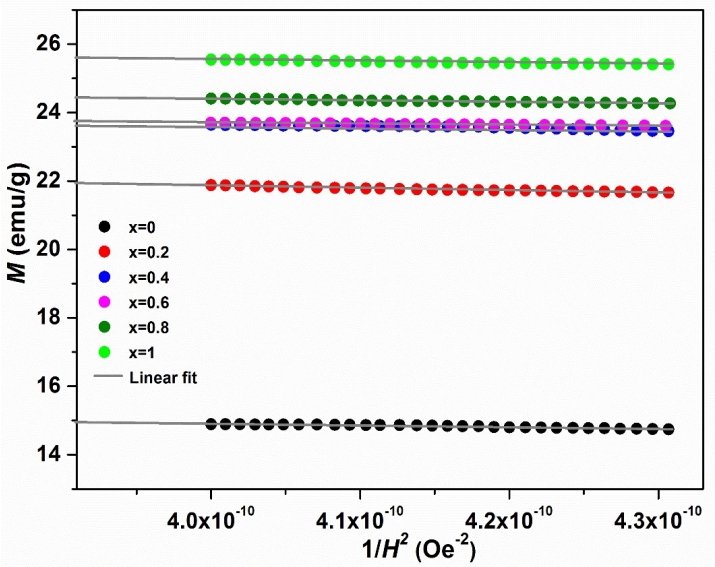

Figure 7.5 *M vs $1/H^2$ plot with linear fit for $SrFe_{8-x}Al_4Zn_xO_{19}$ ($0 \leq x \leq 1$) hexaferrites.*

The coercive field in an M-type hexaferrite strongly depends on the magnetic field, which is required to overcome the magnetic anisotropy barrier. Any variation in magnetic anisotropy needed an external magnetic field for variation in the spin reversal process, which changes the H_c values too. As shown in Table 7.5, the variation pattern of H_c follows the varying trend of H_a. H_a is the physical origin of coercivity, which signifies the maximum limit of H_c that can be attained in a material. H_c is always less than H_a due to particle aggregation (causes self-demagnetization), Brown's paradox, and the existence of

various defects in the system (Gorbachev et al., 2021). The incorporation of smaller Al^{3+} (0.51 Å, $0\mu_B$) ions at Fe^{3+} site will cause the lattice distortion and introduce the microstress, which results in the enhancement of both H_a and H_c (Wang et al., 2012). Hence, a large value of H_c is observed in the compositions. For small Zn^{2+} ion substitution (x = 0.2), enhancement in both the parameters M_s and H_c is observed. It might be possible that some Zn ions also occupy *2b* site for x =0.2, which significantly contributes to H_a and hence H_c of hexaferrtie magnets. Theoretically, H_c is affected by many parameters like particle size and morphology, nature of substituted elements, synthesizing parameters, structural behavior, density of material, and various defects in the system (Ram, 1990). All these factors are present in H_c determination, and the dominancy of one factor over another may cause the variation in magnetic properties as observed in the samples. The substitution of larger and non-magnetic Zn (0.74 Å, $0\mu_B$) ions at Fe^{3+} site results in the reduction of superexchange interaction coupling between Fe ions and hence, reduction in H_a (Banihashemi et al., 2021). The reduction in H_a and improvement in M_s is the reason for decreasing coercivity behavior with the Zn content. Also, a consistent increase in grain size is observed in the microstructural study, which may be the reason for the obtained pattern of H_c value.

7.2.5 Dielectric Properties

Frequency-dependent characteristics of dielectric constant (ε) and dielectric tangent loss ($tan\delta$) are recorded at room temperature for $SrFe_{8-x}Al_4Zn_xO_{19}$ ($0 \leq x \leq 1$) and shown in Fig. 7.6 and Fig. 7.7, respectively. The values of dielectric parameters (ε, $tan\delta$) at 1 MHz frequency are listed in Table 7.6. The variation in dielectric constant with frequency represents the typical ferrite characteristics of ε, i.e., a decreasing pattern of ε with frequency.

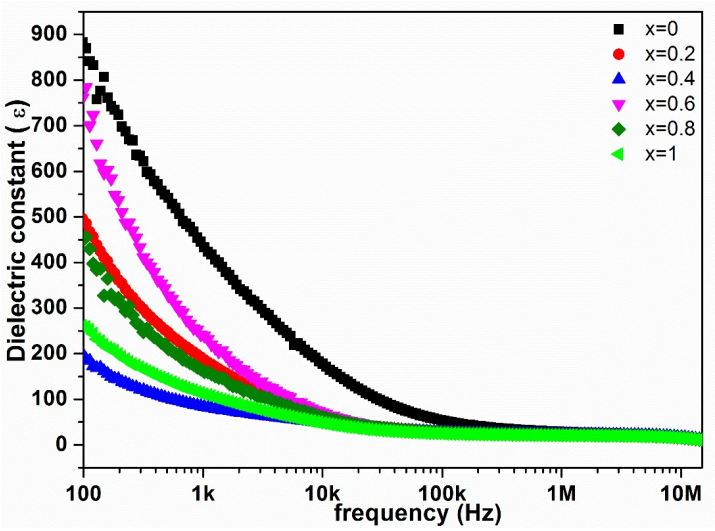

Figure 7.6 *Dielectric constant (ε) of $SrFe_{8-x}Al_4Zn_xO_{19}$ ($0 \leq x \leq 1$)hexaferrites with respect to frequency at room-temperature.*

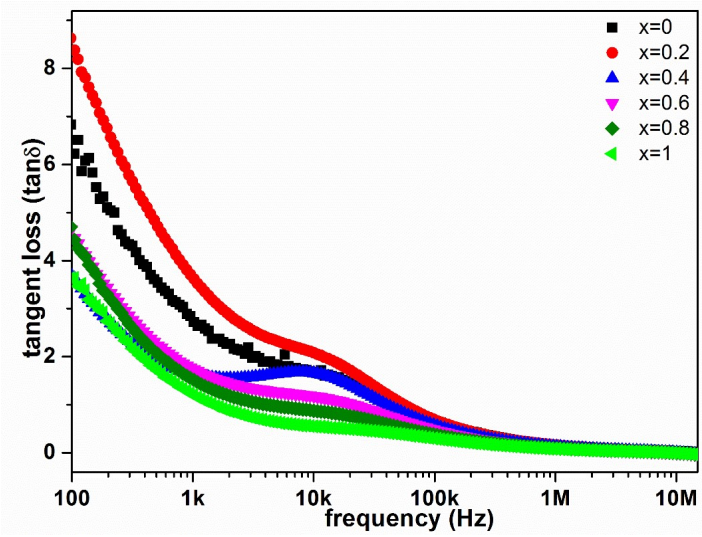

Figure 7.7 *Dielectric loss (tanδ) of $SrFe_{8-x}Al_4Zn_xO_{19}$ ($0 \leq x \leq 1$)hexaferrites with respect to frequency at room-temperature.*

The dispersion phenomena are the origin of dielectric properties in hexaferrite due to interfacial dipole polarization (according to the Maxwell-Wagner model) and intrinsic dipole polarization (according to the Koop model). Maxwell-Wagner model is based on the hypothesis that the dielectric polarization mechanism is similar to the conduction process. The space charge polarization arises due to inhomogeneity in the structure of a material and is the basis for variation in dielectric properties (Ashiq et al., 2009). Koop model

describes that the structure of hexaferrite is made up of two layers: the large first layer consists of grains (conducting layer), and the thin second layer consists of grain boundaries (poorly conducting layer) (Shakoor et al., 2014). At lower frequencies, values of the dielectric constant are large, which is caused by the hopping of electrons that can easily follow the applied field in these frequencies range and results in large polarization. The predominance of oxygen vacancies, Fe^{2+} ion concentration, and grain boundary defects also contribute to the large value of ε at lower frequencies (Dar et al., 2010). Due to the transfer of electrons among Fe^{3+} and Fe^{2+} ions, limited local electron displacement occurs in the applied field direction, which determines polarization. Polarization decreases with increasing frequency, and electron hopping between Fe ions could not follow the applied field because space charge polarizations require a finite time to reorder their axes in the direction of the applied field. It results in a decaying pattern of ε, which becomes almost constant due to the occurrence of only local charge polarization at higher frequencies. During the sintering process, some oxygen ions are expected to be lost due to high processing temperatures. Therefore, some Fe^{3+} ions are expected to transform into Fe^{2+} to maintain charge neutrality. Fe^{2+} ions always have a tendency to occupy octahedral lattice sites, and the electron hopping between Fe^{3+} and Fe^{2+} at this site is mainly responsible for the conduction mechanism in hexaferrite. Substitution of Al^{3+} ions prefers the octahedral site and forces Fe^{3+} ions of octahedral sites to migrate to the tetrahedral site. It decreases Fe^{3+} ions at the octahedral site and results in the decrease of dielectric constant value in comparison to pristine SrM. Substitution of Zn^{2+} ions prefers the tetrahedral site, which increases the concentration of Fe^{3+} ions at the octahedral site by forcing to transform Fe^{2+} ion into Fe^{3+} in order to maintain charge neutrality in composition. The reduction of Fe^{2+} ion concentration at the octahedral site by Zn^{2+} substitution and the reduction of Fe^{3+} ion

concentration at the octahedral site by Al^{3+} substitution collectively reduce the dielectric constant value by reducing the electrical conduction of charge carriers.

In dielectric materials, some losses arise from work-done required to overcome the frictional damping forces exerted by the dipole rotation (Ashiq et al., 2009) and energy loss due to domain wall resonance. The dielectric tangent loss ($tan\delta$) of hexaferrite generally shows a decreasing behavior with increasing frequency. Grain boundaries are the dominant entities in the lower frequency range, while grains are dominant entities in the higher frequency regions. Due to the poorly conducting thin layer of grain boundaries, high energy is required for electron hopping which results in the high $tan\delta$ in the low-frequency region. At higher frequencies, energy losses are low since domain wall motion is suppressed, and magnetization is forced to change rotation (Dar et al., 2010). The dominance of grains with the increasing frequency reduces the required energy for the transfer of electrons between Fe ions and results in the observed characteristic of $tan\delta$. According to the microstructural study, an increase in average grain size with the substitution of Zn^{2+} ions results in the reduction of conduction losses and hence, the decline of $tan\delta$ value with the Zn amount.

Table 7.6 *Room-temperature value of dielectric constant (ε), tangent loss ($tan\delta$), resistivity (ρ), and conductivity (σ) of $SrFe_{8-x}Al_4Zn_xO_{19}$ ($0 \leq x \leq 1$)hexaferrite at 1MHz frequency.*

Composition	ε	$tan\delta$	ρ (10^6 Ω-cm)	σ (10^{-7} S-cm^{-1})
x=0	28.67	0.161	37.96	26.34
x=0.2	24.53	0.158	45.10	22.17
x=0.4	23.74	0.129	57.02	17.54
x=0.6	23.40	0.112	66.54	15.03
x=0.8	22.23	0.094	83.16	12.03
x=1	20.59	0.079	106.7	9.37

7.2.6 Electrical Properties

Fig. 7.8 shows the frequency-dependent ac-resistivity behavior of $SrFe_{8-x}Al_4Zn_xO_{19}$ ($0 \leq x \leq 1$) hexaferrites at room temperature. The value of ac-resistivity (ρ) and ac-conductivity (σ) at 1 MHz frequency are listed in Table 7.6.

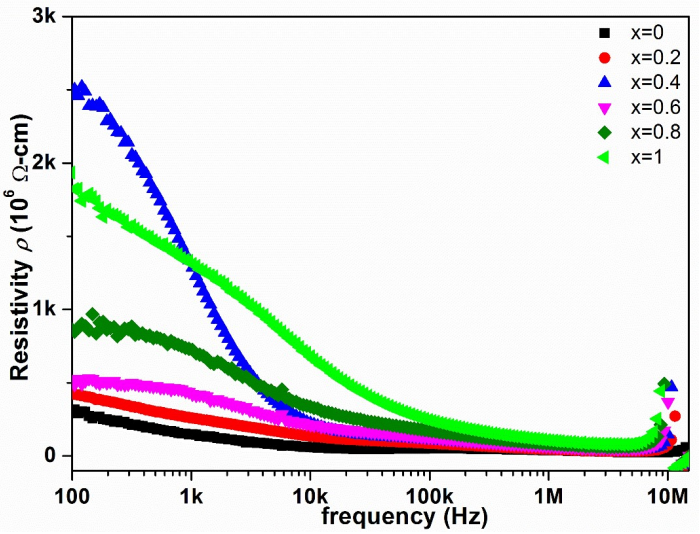

Figure 7.8 *Frequency-dependent resistivity variation in $SrFe_{8-x}Al_4Zn_xO_{19}$ ($0 \leq x \leq 1$) hexaferrites.*

Electrical conduction is an increasing function with frequency if the conduction is caused by electron hopping, while it is a decreasing function with frequency if the conduction is caused by band conduction (Dar et al., 2010). Electron hopping between Fe^{3+} and Fe^{2+} at the octahedral sites is mainly responsible for electrical conductivity in hexaferrite (Bellad & Chougule, 2000); hence, decreasing behavior of resistivity (inversely proportional to conductivity) is observed for compositions. The decreasing characteristic of resistivity with frequency can be described based on the pumping force of applied field frequency that promotes the transfer of charge carriers between different localized states and also liberates the trapped charges in a system. These charge carriers contribute to the conduction mechanism along with the simultaneously produced electrons due to valance exchange between Fe ions and increase the conductivity by reducing the resistivity with

frequency. The reduction of Fe^{2+} ion concentration at the octahedral site due to Zn^{2+} ion substitution and the reduction of Fe^{3+} ion concentration at the octahedral site by Al^{3+} ion substitution collectively reduce the electron hopping between Fe^{3+}-O-Fe^{2+} at the octahedral site, which reduces the conduction mechanism in the composition. Hence, an increasing resistivity value is observed in the compositions with the Zn ion content.

7.3 Conclusions

A composition of $SrFe_{12-x}Al_4Zn_xO_{19}$ (x = 0, 0.2, 0.4, 0.6, 0.8, 1) was effectively synthesized by sol-gel auto-combustion method. Structural, magnetic, and dielectric studies were carried out to see the effect of substitutional elements. It can be concluded by the magnetic study that Al^{3+} ions have a great significance in improving the H_c value of SrM magnets even higher than NdFeB. The effect of Zn^{2+} ion is more prominent in improving the M_s of compositions but at little expense of H_c. An improvement in both M_s and H_c is observed for small Zn^{2+} ion content (x = 0.2). For the $SrFe_{7.8}Al_4Zn_{0.2}O_{19}$ composition, a large H_c ~18.51 kOe is observed with M_s ~21.87 emu/g. It causes a good improvement in the magnetic properties of rare-earth free SrM-based magnets. In addition to such magnetic properties, these magnets also offer high resistivity, negligible eddy current loss, high oxidation & corrosion resistance, which is practically desirable for efficient PM applications. The current progress in the magnetism of the SrM-based hexaferrites suggests that the large-scale involvement of these magnets is possible in different areas of permanent magnet applications.